Soft Matter

Accepted Manuscript

This article can be cited before page numbers have been issued, to do this please use: A. Rath, P. M. Geethu, S. Mathesan, D. K. Satapathy and P. Ghosh, *Soft Matter*, 2018, DOI: 10.1039/C8SM00042E.

ROYAL SOCIETY OF CHEMISTRY

rsc.li/soft-matter-journal

View Article Online
DOI: 10.1039/C8SM00042E

Journal Name

ARTICLE

Solvent Triggered Irreversible Shape Morphism of Biopolymer Films

Received 00th January 20xx,
Accepted 00th January 20xx

DOI: 10.1039/x0xx00000x

www.rsc.org/

Amrita Rath[a], P.M. Geethu[b], Santhosh Mathesan[a], Dillip K. Satapathy[b] and Pijush Ghosh[a]*

We report controlled reversible and irreversible folding behavior of biopolymer film simply by tuning the solvent characteristics. Generally, solvent triggered folding of soft membranes or film is succeeded by unfolding. Here, we show that this unfolding behavior can be suppressed/delayed or even completely eliminated by altering the intrinsic nature of the solvent. A reversible folding of biopolymer film is observed in response to water, whereas, an irreversible folding in the presence of an aromatic alcohol (AA) solution of different molar concentration is reported. The folding and unfolding behavior originates from the coupled deformation-diffusion phenomena. Our study indicates that the presence of an AA influences the relaxation behavior of polymer chains, which in turn affects the release of stored strain energy during folding. Controlling the reversibility as well as the actuation time of biopolymer film by tuning the solvent is explained in detail at bulk scale by applying appropriate experimental techniques. The underlying mechanism for the observed phenomena is complemented by applying simulation study for a single polymer chain at the molecular length scale. These solvent-triggered hygromorphic response of biopolymer film has a huge potential as a sensor, soft robots, drug delivery, morphing medical devices and biomedical applications. We provide experimental evidence about the weight lifting capacity amounting to ~200 times of its own weight for permanently folded membranes.

Introduction

The stimuli responsive biopolymers with advanced functionalities have found a wide range of futuristic applications as soft actuators[1], morphing medical devices[2–4], artificial muscles[5] and implants[6], soft robotics[7–9], sensors[10,11], drug delivery[12–14] and many more. Different soft polymers such as shape memory polymer, electroactive polymer, elastomers and hydrogels are gaining much attention as shape changing materials owing to their large deformability, wider range of mechanical properties, sensitivity to different stimuli, excellent biocompatibility and many more features[15]. Numerous strategies to realize the three dimensional shape change of these polymers includes matrix modification, controlling surface topography[15], localized or external photo effect[16], differential swelling[17,18], inclusions, hole programming[19], hybrid bilayers[20], unbalanced thermal shrinkage[21], capillary forces[22] etc. All these methods are suitably exploited depending on specific utility.

Here we report controlling the reversibility of the biopolymer film by suitably designing the triggering solvent. This strategy provides a promising insight into the designing of both reversible and irreversible/permanent folding behavior as well as a transition from reversible to irreversible folding and vice versa of the same biopolymer film with solvents. Moreover, it offers the possibility of having a control over the actuation speed, rate and time of folding. The folding is due to differential swelling across the thickness of the film. During folding, the polymer chains at the bottom layer experience tension, whereas the top layer chains are in compression. With the passage of time, water diffuses further through the layers of the film thus, relaxing the polymer chains to restore their equilibrium or preferred state. This relaxation is indicated through unfolding phenomena of the film. However, the unfolding process is strongly affected in the presence of another solvent, i.e. aromatic alcohol (AA), which causes the film to undergo a permanent folding behavior. Interestingly, the permanent shape can be made reversible as and when required by altering the solvent characteristics. Further, the AA solution affects the folding behavior in terms of time and speed of folding. Thus, solvent controlling both reversibility as well as the actuation time of the folding behavior is a novel concept which has a tremendous potential in advanced therapeutic applications.

In our previous work[17], we have reported that the cross-linking of the pristine chitosan film is an efficient means for a controlled and predictable pathway of folding while demonstrating its application as a possible sensor and soft

[a] Nanomechanics and Nanomaterials Laboratory, Solid Mechanics Group, Department of Applied Mechanics and Soft Matter Center, Indian Institute of Technology Madras, Chennai-600 036, Tamil Nadu, India.
[b] Soft Condensed Matter and Biological Physics Laboratory, Department of Physics and Soft Matter Center, Chennai-600 036, Tamil Nadu, India.

† Footnotes relating to the title and/or authors should appear here.
Electronic Supplementary Information (ESI) available: MOV_1: Flower shaped opening and closing of the film; MOV_2: Reversible and irreversible folding of film; MOV_3: Twisting of film; MOV_4: Valve like opening of the film; MOV_5: Pulling of single polymer chain during SMD; S.1:Experiment methodology details.See DOI: 10.1039/x0xx00000x

View Article Online
DOI: 10.1039/C8SM00042E

cargo. In this report, we utilize the similar cross-linked chitosan film and demonstrate the possibility of having both reversible and irreversible folding of the film with aromatic alcohol (AA) medium as a trigger solvent. By changing the molarity of the solvent, the reversibility is observed to be affected and at a critical molar concentration, the film undergoes a permanent folding. We have made an effort to understand the underlying mechanism behind this irreversible folding behavior at different length scales by applying experimental techniques, such as dielectric relaxation spectroscopy (DRS) and molecular mechanistic study (Molecular Dynamics).

Results and discussion

Reversible Folding

A hygromorphic response of cross-linked chitosan film is demonstrated by placing the film on water surface as shown in Fig. 1. The self-folding behavior is observed only when one side (bottom surface) is exposed to water contact due to differential swelling across the thickness of the film. Diffusion gradient is the primary driving force behind this folding phenomenon. The differential water volume at the bottom layer compared to its immediate top counterpart leads to the curvature. The diffusion of water alters the mechanical stiffness of the matrix, which in turn influences the diffusion behavior of the polymer.

Thus, the self-folding phenomena of the film is a coupled diffusion-deformation phenomenon. The film in Fig. 1a can be assumed to be dissected to various layers named as Li-1, Li and Li+1 with water content (W) varying in a decreasing order as Wi-1 > Wi > Wi+1 respectively, at any particular instant of time during folding. In the folded stage, the polymer chains exists in compressive strain and tensile strain state in two consecutive top layer L_i and bottom layer L_{i-1}, respectively. With further diffusion of water, chains in layer L_i changes from compressive to tensile state and so also the other consecutive layers. This continues across the thickness until the entire structure folds and overall compression and tensile regions are separated by the neutral axis of bending as shown in Fig. 1c. During folding, the effect of diffusion gradient predominates; however, as this gradient reduces with more absorption of solvent, the relaxation phenomena takes over causing the film to unfold. The presence and interaction of water molecules at the proximity of the chitosan functional group facilitates the necessary conformational changes of the polymer chains. As a result, the strain energy stored due to bending or complete folding is released by the film through the phenomenon of unfolding.

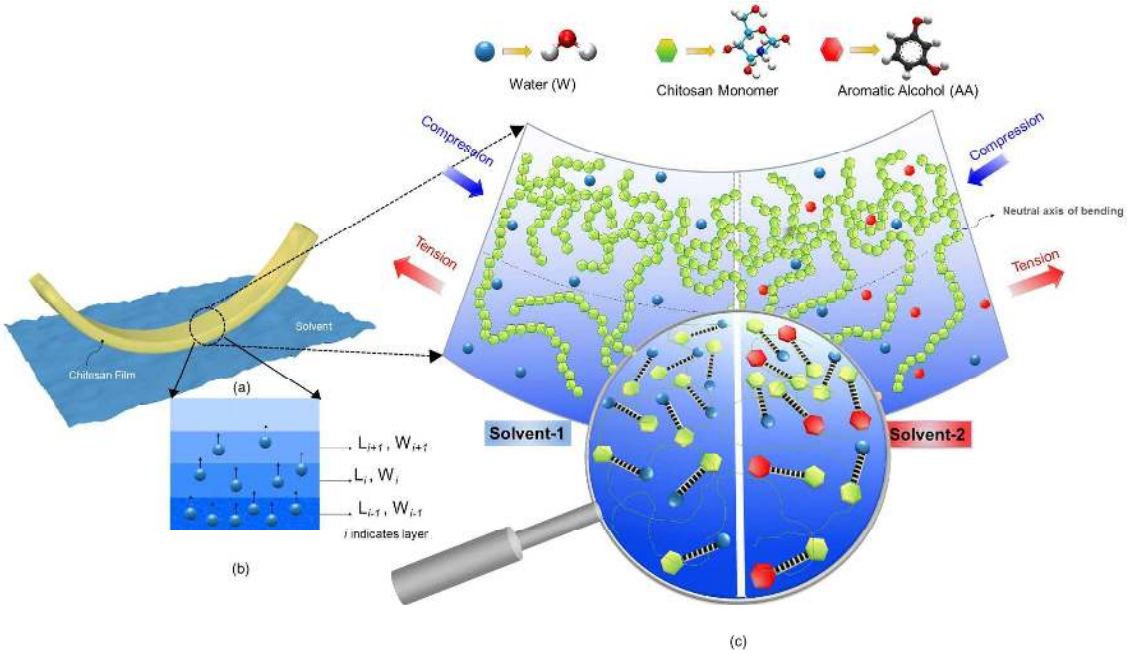

Fig. 1 (a) Schematic representation of the folding of the film due to water diffusion (b) at any particular instant of time during folding, a portion of the film thickness can be visualized to be disintegrated into different layers with varying water content represented by L and W respectively, and (c) during folding, the polymer chains in bottom region under tension and top region in compression state with a zoomed in view showing all the possible interactions between chitosan, aromatic alcohol and water molecules.

Irreversible/Permanent Folding

The permanent folding behavior is observed for CS films in response to AA solution. This is due to the modification of the diffusion characteristics of the solution through alteration of polymer chain conformation. This reduces the degree of freedom of the polymer chain thus leading to irreversible behavior.

View Article Online
DOI: 10.1039/C8SM00042E

The underlying mechanism responsible for this behavior is explained in detail in the subsequent sections. The folding behavior of thin film is studied at different length scale to gain comprehensive understanding of the phenomena. In this study, the focus is on addressing both the bulk scale as well as the molecular scale mechanism affecting the folding behavior. Dielectric spectroscopy experiments (DRS) are performed to measure the response of the polymer chains to solvents, quantified by the polymer chain segmental mobility, which affects the properties of polymer in bulk. At the molecular scale, the reason behind the stiffness variation is understood by performing molecular dynamic simulation (MD) study.

Characterization of Permanent Folding

This article focuses primarily on the irreversible nature of folding triggered by appropriately designed solvent medium. Our previous work explains in detail the reversible and path controlled self-folding behavior of chitosan biopolymer film in response to water[17]. Few examples of various permanently acquired shapes of chitosan films upon exposure to the solvent are demonstrated in Fig. 2. Each of these permanent folding has reversible counterpart depending on applied trigger solvent characteristics (Refer MOV_1 to MOV_4 in supplementary video). The rational behind choosing resorcinol (aromatic alcohol) as a trigger solvent was to study the competitive interaction with water which has also a similar reactive -OH group that form H-bond with the reactive sites of chitosan, thus affecting the folding behavior. Resorcinol being one of the simplest aromatic alcohols which closely resembles OH group and benzene ring in amino acids was thus applied, also keeping in mind the extension of this study in future to biological molecule.

The permanent folding is further dependent on the molarity of the AA solution. With an increase in the molarity of the solution, the diffusion process gets slowed down, reducing the rate of folding ($d\theta/dt$) and thus increasing the actuation time of folding as shown in Fig. 3. The folding rate during the entire span of folding is observed to be non-uniform. In case of reversible folding, the complete folding of the film is followed by unfolding phenomena, tracing back the same pathway of folding. However, at and above a critical molar concentration (4M), the film does not unfold and thus permanently retains its shape even after the removal of the trigger solution.

The folding behavior of the film is characterized further by its responsiveness to the solvent or triggering medium. In this case, it is calculated till both ends of the film connect to each other as shown schematically in Fig. 4. The responsiveness is experimentally measured by the total folding time (T) which is the sum of i) response time T_1 and ii) initiation of the folding to end of folding time T_2 as shown in Fig. 4.

T_1 is the time taken for the film to initiate folding from the point it is placed on the solution. This time T_1 primarily depends on the occupancy of the available free sites at the film surface by solvent molecules, whereas, T_2 is dependent on the overall diffusion characteristics of the film matrix. The total time T, increases with an increase in the molarity of the solution varying in the time scale between 20 s to 100 s. As

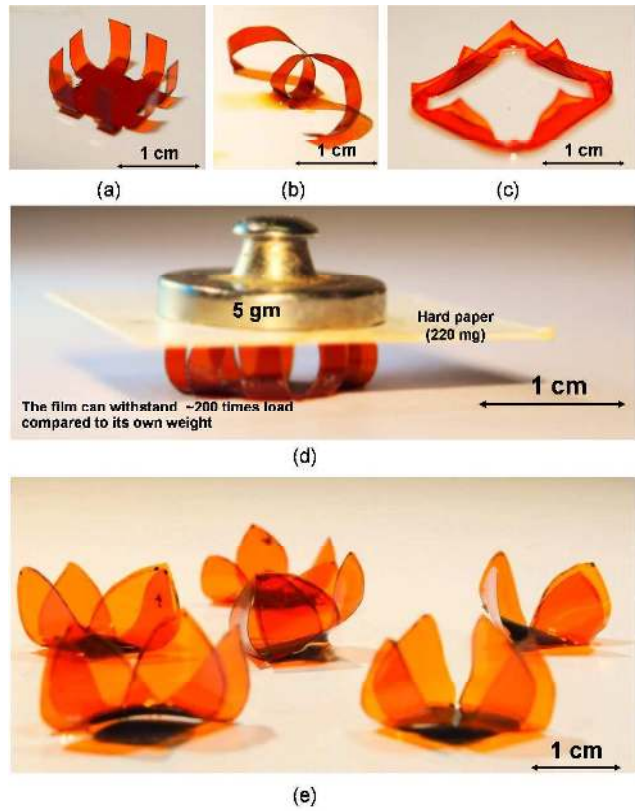

Fig. 2 Snapshots of permanently acquired folded structures in response to solvents, (a) and (b) load carrying folded structure, (c) twisting effect, (d) opening and closing of valve and (e) flower shaped folding (Attached supplementary videos).

observed from the experiments, the response time, T_1 gradually increases with the increase in molarity till the critical concentration is reached, beyond which there is no further increase in T_1. The primary contribution of folding comes from time T_2, which gets affected significantly with increasing molarity.

The reason behind increasing time T_2 with increasing molarity is due to the number of available water molecules to interact with the reactive groups of chitosan chains. It starts reducing as a result of increased interaction with AA molecules which is explained in detail later in the mechanism section. One deviation is observed for reported time T_2 for 8M, which is found to be less compared to T_2 of 6M. This is because the extent of folding or folding curvature reduces with higher molarity, thus measuring lower folding time. It is to be noted that the reversibility of the film can be restored by appropriately lowering the concentration of AA as and when necessary.

View Article Online
DOI: 10.1039/C8SM00042E

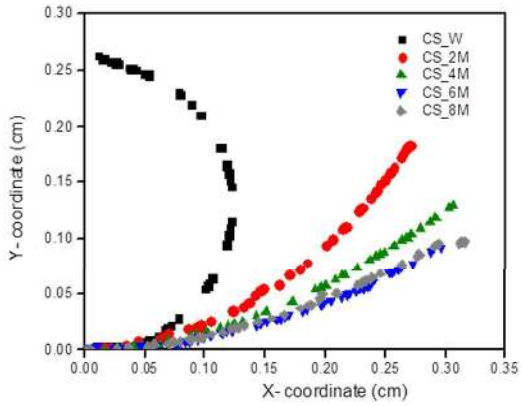

Fig. 3 A graph showing *x* and *y* coordinate of the film folding at T_2= 20 s. As observed, at a given time, the folding decreases as molarity of the solution increases.

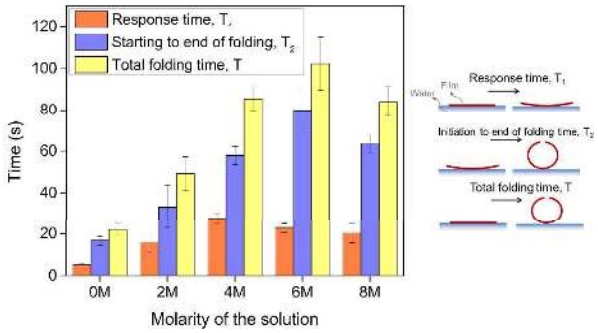

Fig. 4 A plot showing the effect of molarity on the time of the folding of the film.

Apart from folding behavior characterization, the mechanistic understanding of the pristine and cross-linked chitosan film is important for designing purpose. The depth sensing nanomechanical characterization is performed to determine the material Young's modulus (*E*) and hardness (*H*). The *E* and *H* values obtained for pristine CS and cross-linked CS film are 1.49 ± 0.07 GPa and 0.11±0.01 GPa and 3.08 ± 0.15 GPa and 0.21 ± 0.005 GPa respectively. Owing to the small dimension of the film in the actual field of use and higher spatial resolution, quasi-static nanoindentation is a convenient technique compared to bulk mechanical characterization. The detailed method of nanoindentation is reported in our previous papers[23,17].

Irreversible/Permanent Folding Mechanism

Dielectric Relaxation Spectroscopy (DRS)

Dielectric relaxation spectroscopy provides information on segmental mobility and relaxation dynamics of polymers as a function of the frequency of applied AC voltage. The response of the polymer is derived from the interaction of the electric dipoles present in the polymer chain with the applied alternating electric field and the resulting relaxation kinetics.

For a dry chitosan film, a dielectric relaxation is observed in the frequency range from 10 Hz to 10 kHz at room temperature (~27 °C) and is attributed to the β-process which is associated with local motions of side groups in chitosan[24,25]. The water present in chitosan leads to devitrification and enhances the segmental mobility of chitosan polymer chains[26,27]. The observed β-relaxation in chitosan-water complex is modeled using Cole-Cole function[28,29] given by Eq. (1)

$$\varepsilon^*(\omega) = \varepsilon_\infty + \frac{\Delta\varepsilon}{1+(i\omega\tau)^\alpha} + \frac{\sigma_{DC}}{i\omega\varepsilon_0} \qquad (1)$$

where, ε_∞ is the real part of permittivity at high frequencies, τ is the characteristic relaxation time, Δε dielectric relaxation strength and σDC is the dc-conductivity of the system. The asymmetric broadening parameter α usually assume a value in the range 0<α<1. The fitting parameters obtained using Eq. (1) for chitosan film are given in Table 1.

Next, segmental mobility and relaxation dynamics of chitosan polymer films are investigated in the presence of different molar concentrations of AA. The frequency dependence of real and imaginary part of dielectric permittivity for chitosan films with four different molar concentrations of AA, i.e. 2M, 6M, 8M and 10M are shown in Fig. 5. The measured spectra are again fitted with Cole-Cole function given by Eq. (1) and the parameters obtained from fit are tabulated in Table 1. In the presence of AA molecules, a decrease in β-relaxation time (τ) of chitosan polymer chains is observed as compared to that of chitosan chains in the absence of AA molecules.

This clearly suggests an increased segmental mobility of chitosan polymer molecules in the presence of added solvent. Also, an increase in τ is observed with the increase of molar concentrations of AA as represented in Fig. 6a, indicating a decrease in the segmental mobility of the chitosan polymer chains. In other words, mobility of chitosan chains diminishes upon increasing AA concentration.

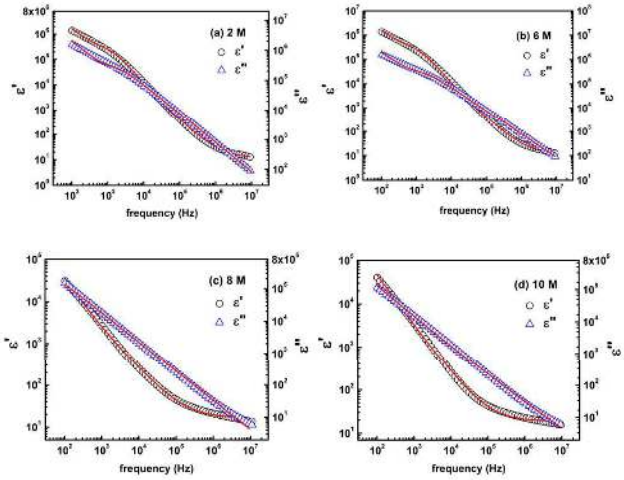

View Article Online
DOI: 10.1039/C8SM00042E

Fig. 5 The real and imaginary part of dielectric permittivity plotted as a function of frequency for chitosan films with (a) 2M AA-water solution, (b) 6M AA-water solution, (c) 8M AA-water solution and (d) 10M AA-water solution. The symbols show the measured dielectric data and solid lines show the fits according to Eq.(1).

Alternatively, the change in relaxation time of polymers can also be observed by measuring the electrical modulus (M* = M´ + iM") as a function of frequency. The imaginary part of M* for chitosan polymer films with different concentrations of AA is shown in Fig. 6b. The peak value of M" shifts towards lower frequency with increase in AA concentration, which provides model-independent and direct evidences for the decrease in relaxation time with increase in AA concentration. This further supports the decreased segmental mobility of chitosan chains and the associated stiffening of chitosan polymer chains in the presence of AA-water solvent.

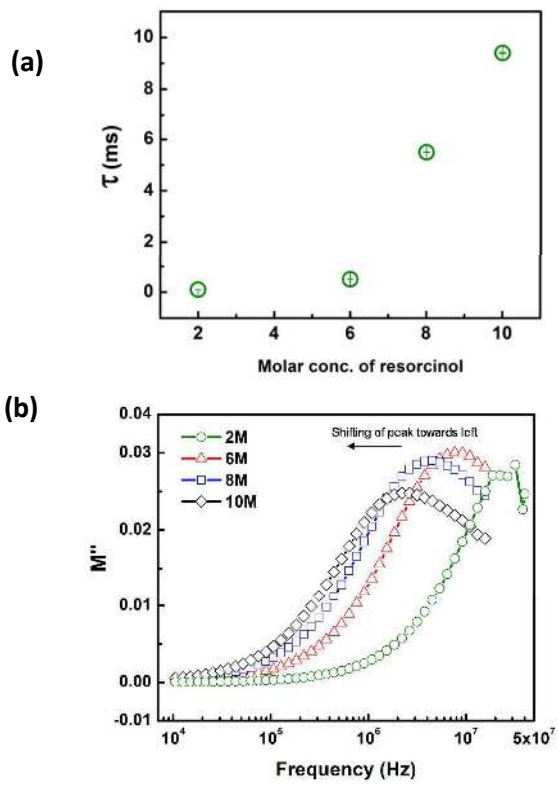

Fig. 6 (a) The β-relaxation time τ for chitosan polymer chains with different molar concentrations of AA-water solutions and (b) Frequency dependence of the imaginary part of dielectric modulus M" for chitosan polymer with four different molar concentration of AA solution given as 2M, 6M, 8M and 10M. The shifting of peak in M" towards lower frequencies with increase in molar concentrations of aromatic alcohol is shown.

Sample	ε_∞	$\Delta\varepsilon$	τ (s)	α
Chitosan film	3.7	9.7e+1	4.9 e-3	0.64
Chitosan+AA (2M)	3.4	3.9e+5	9.7e-5	0.96
Chitosan+AA (6M)	10.9	3.7e+5	5.1e-4	0.95
Chitosan+AA (8M)	14.4	3.2e+5	3.5e-3	0.90
Chitosan+AA (10M)	18.2	1.2e+5	4.4e-3	0.89

Table 1. Fitting parameters ε∞, Δε, τ, α and β obtained using Eq. (1) for chitosan film and chitosan with four different molar concentrations of AA solution given as 2M, 6M, 8M and 10M.

Molecular Dynamics Study (MD)

The phenomena taking place at the bulk scale is the consequence of sequences of events at the molecular scale. Therefore, a MD study has been performed to understand the underlying molecular mechanism in response to solvent medium and address its bulk scale phenomena affecting the reversibility of the folding. A single polymer chain unfolding is modeled to get an insight into the fundamental molecular interaction with and without the presence of AA molecules. Stiffness is one of the contributing factors responsible for reduced chain flexibility, which is also measured at bulk scale applying DRS study. Further, MD study is applied to discuss on the molecular origin of difference in the chain stiffness by analyzing the chain dynamics using radial distribution function (RDF), dihedral angle variation and analyzing the strength of H-bond. The steered molecular dynamics provides the detailed information associated with molecular deformation mechanics from the obtained force-displacement (F-D) profile. The slope obtained from the F-D profile can be considered to be a quantitive measure of the stiffness of the polymer chain. During pulling, this stiffness originates from the molecular conformation and non-bonded interaction with the atoms at closer proximity[30].

Stiffness of the model system

The load carrying behaviour of a single polymer chain system is analyzed by pulling it in X-direction (Refer MOV_5 in supplementary video). The PBC of the system is appropriately considered. The chain is elongated up to a distance of about 30% of the molecular strain. [Strain = $(\Delta L/L_0) \times 100$; $\Delta L = L_t - L_0$, where, L_t= molecular length at time, t and L_0 is the initial length]. The stiffness of the polymer chain is calculated from slope of the F-D plot in the range between 5-15% strain for all the simulation models. In this study, initial length, L0 is measured to be 350 Å. A representative F-D plot for CS-Water and CS-20M model is shown in Fig. 7 to compare the slope of the plot. The stiffness value of the single polymer chain for different solvent system has been reported in Table 2. The values are the average of three simulations from different initial structures. The results suggest gradual stiffening of the polymer chains with increasing molarity of the AA solution. The stiffness is primarily the measure of resistance to deformation in response to any externally applied force. The stiffness (s) of the single polymer chain at the molecular scale affects the overall polymer matrix stiffness (K) at the bulk scale. The stiffening of the polymer chains arises or varies due to different conformational arrangement of the molecules. This arrangement can be categorized as spatial and temporal conformations which includes the intramolecular hydrogen network[31] belonging to former category and the frequency of forming and breaking of H-bonds belonging to later category.

View Article Online
DOI: 10.1039/C8SM00042E

Sl. No.	Model Type	Stiffness (pN/Å)	Maximum Load (pN)
1	CS	31 ± 4	700
2	CS-Water	17 ± 3	1000
3	CS-2M	32 ± 11	1200
4	CS-10M	37 ± 4	1700
5	CS-20M	57 ± 7	2000

Table 2. The stiffness value and the maximum load carrying capacity of all the simulation models.

The interaction of reactive groups between water, AA molecules with chitosan chain locally modifies the flexibility of the chain by hindering the rotational degree of freedom which is quantified by variation in the dihedral angle. The increase in the stiffness of the chain is the consequence of the reduced variation in the dihedral angle and vice versa. The dihedral angle variation of the CS chain is measured to be less in the presence of AA molecules as compared to water from MD study. Thus, indicating stiffer polymer chains in the presence of AA, i.e. $s_{(aromatic\ alchol)} > s_{water}$. These are the localized molecular phenomena observed throughout the matrix due to the preferential interaction of AA with the chains. The overall effect of these localized phenomena when transformed on a global scale can be envisioned to be a contributing factor for the continuum scale stiffness, qualitatively represented by linear spring stiffness K. This indicates a stiffer polymer matrix in the presence of AA molecules, i.e., $K_{(aromatic\ alcohol)} > K_{water}$.

A consistent trend both at molecular as well as bulk scale is observed for the stiffness of the polymer chains in the presence of AA and water molecules. A detailed analysis of dihedral conformation and its angle variation is presented in the subsequent sections.

The other important factor is the strength of the H-bond between chitosan–water and chitosan–AA model. It provides an insight into the competitive interaction between water and AA molecule to have more affinity to form H-bond with chitosan chain and thus, affecting the chain stiffness as discussed above.

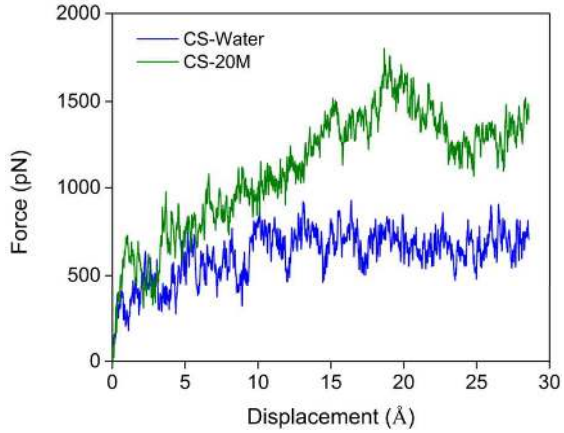

Fig. 7 A force-displacement plot obtained from SMD simulation for CS-W and CS-20M model with spring stiffness, k=7 kcal/mo/Å^2 and pulling velocity, v = 0.5 Å/ps.

H-bond Analysis

H-bond analysis is performed to examine the dynamics of the water molecules in the polymer system. The amine and the hydroxyl group present in chitosan polymer are the main reactive sites for H-bond formation with hydroxyl group of water and AA molecules. The radial distribution function (RDF) between two atoms gives the probability of finding a particle at a distance *r* from the reference point. Of all the reactive sites examined, the most prominent peak is observed between O_6 of chitosan and H of water as shown in Fig. 8a. Therefore, the number of H-bond is calculated between these two atoms and compared with all the models for further analysis. To analyze the strength of the hydrogen bonding, H-bond analysis is performed as a function of hydrogen bond distance, r_{AD} (A:acceptor atom; D:donor atom) and geometry as angle, θ between hydrogen atom and a highly electronegative atom (O in this case). The hydrogen bonds are divided into high, medium and low depending on donor and acceptor atom[32–34]. A bond distance r_{AD} < 2.8 Å and θ < 20˚ is defined as high strength H-bond, r_{AD} < 3.2 Å and θ < 30˚ as medium strength H-bond and r_{AD} < 4 Å and θ < 40˚ as low strength H-bond.

The number of hydrogen bonds formed of varying strength is shown in Fig. 8a. In a similar way, RDF between all the reactive sites present in chitosan and AA molecules is analyzed. A prominent peak is observed for H in OH of AA with O_6 of chitosan polymer. Thus, the number of H-bond is calculated between these two atoms as shown in Fig. 8b. The presence of AA molecules largely affects the dynamics and molecular behavior of the chitosan polymer. Fig. 8a suggests a reduction in the interaction between chitosan and water with increase in the molarity of the AA solution. The reactive sites in chitosan interact with AA solution through formation of hydrogen bond as shown in Fig. 9c, thus replacing the site earlier occupied by a water molecule. A similar complimentary trend is observed in Fig. 8b which shows an increase in the interaction between chitosan and AA. As a result of increased interaction, it can be conceptualized that AA molecules might be acting as a stable hinge between two or more chitosan chains holding the entire network together and affecting the overall chain flexibility as shown in Fig. 9a.

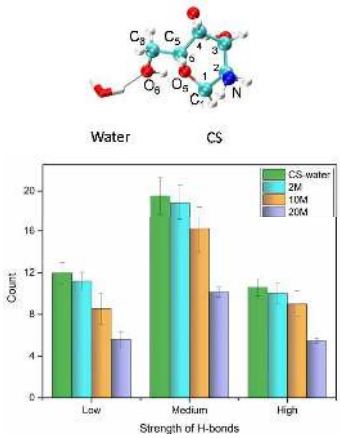

(a)

View Article Online
DOI: 10.1039/C8SM00042E

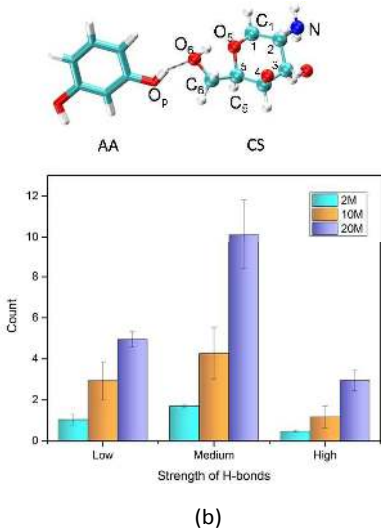

Fig. 8 Number of H-bond counts between (a) O_6 of chitosan with H of water and (b) O_6 of chitosan with H of AA molecule.

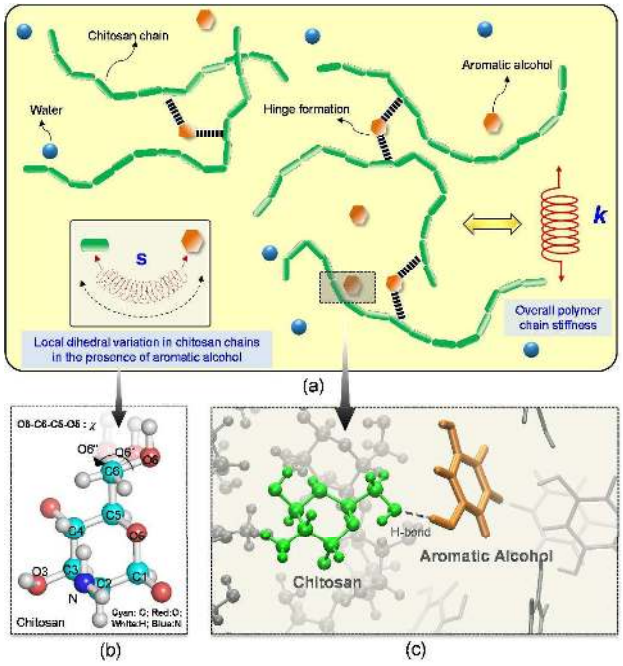

Fig. 9 (a) A schematic showing the matrix consisting of chitosan polymer chains surrounded by water and aromatic alcohol molecules, (b) the variation of dihedral angle in the presence of aromatic alcohol and (c) snapshot from VMD showing the H-bond formation between reactive groups of chitosan and aromatic alcohol.

Next, the analysis of H-bond is performed and represented by the count and strength of the bond. The count of the H-bond shows an increasing trend with higher molar AA solution. To understand a higher affinity of either water or AA towards CS, the number of H-bond between CS and water in the absence of AA and CS-AA for 20M solution is calculated. 20M solution and medium strength H-bond is considered to be a representative case for this count. It is observed that 34% more number of H- bonds is formed between CS and AA molecules as compared to water after normalizing the counts. An increasing trend is observed for all strength of H-bonds, which confirms a higher affinity of AA molecule to interact with the CS polymer. Moreover, medium strength H-bonds is observed to have a higher weightage as compared to low and high strength H-bonds. The increased interaction of the AA solution with chitosan has the potential to affect the dihedral conformations of the chitosan chain. This is examined by calculating the dihedral angle over the trajectories.

Dihedral Angle Variation

The flexibility and mobility of the polymer chain depends on the molecular conformation specified by dihedral angle. Chitosan has three important dihedral angles, χ, Ψ and ϕ that determines its molecular flexibility[35] as shown in Fig. 10. These dihedral angles are directly associated with atoms O_6, and indirectly associated with atoms O_3 and N respectively, thus forming the potential site for H-bond formation. However, the number of H-bond forming between N atom of chitosan with water or AA is relatively less. Therefore, dihedral angle variation is shown for χ and Ψ. The dihedral angle is calculated by using output trajectory obtained during equilibration stage in VMD for an initial time frame of 30 ps. The reason behind choosing an initial time frame is that the hydrogen bond formation is highly dynamic is nature due to continuous making and breaking of bonds.

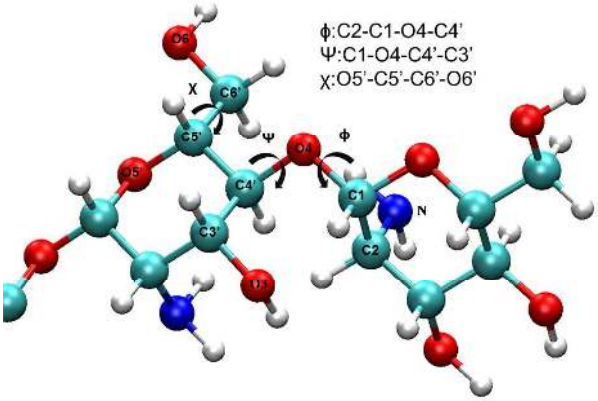

Fig. 10 A snapshot of chitosan chain showing various dihedral angles and the corresponding atoms participating in angle formation[34].

A comparison of dihedral angle variation for CS-W and CS-20M for three representative potential sites for hydrogen bond formation is made. The same site is taken for comparison between the two models. The variation of angle for the entire range of calculation is 74° and 48° for angle χ; 360° and 46° for angle Ψ for CS-W and CS-20M model, respectively. These values are the difference between the maximum and minimum measured dihedral angle. It shows a higher variation

View Article Online
DOI: 10.1039/C8SM00042E

of dihedral angle, χ for CS-W represented by O6"-C6-C5-O5 angle as compared to CS-20M represented by O6´-C6-C5-O5 dihedral angle as shown in Fig. 9b. These variations are even more pronounced for dihedral angle Ψ. The conformational restriction offered by the dihedral angle of chitosan is due to the formation of H-bond between chitosan and AA molecule. This bond might break and reform again with water, thus, chitosan chain gaining back its conformational freedom. Therefore, it is also important to mention that the conformational restriction is not observed for all the potential reactive sites due to dynamic nature of the H-bond formation. So, all the sites are carefully scrutinized by visual inspection and the potential sites showing this variation are selected for the purpose of comparison.

Conclusions

To summarize and conclude, the diffusion gradient across the layer causes the film to fold. The rate of folding depends on the magnitude of this gradient and the stiffness at particular instant of time. The folding induces compressive and tensile stresses which the film tries to reduce through the favorble conformational changes of the chains. During folding, the effect of diffusion gradient predominates; however, as this gradient reduces with more absorption of solvent, polymer tries to move from metastable state to a more stable state, thus causing the film to unfold. The unfolding phenomenon is a mean to release the strain energy stored due to folding. The film in the presence of AA initially folds due to the existence of differential swelling across the thickness. Subsequently, a competitive interaction takes place between AA and water molecules to occupy the site of chitosan. The study shows that AA has more affinity to interact with chitosan as compared to water. This interaction increases the stiffness of the chain which prohibits free movements of polymer chains. The cause of this enhanced stiffness in the presence of AA is studied at two different length scales. The results from DRS experiments suggest reduced mobility with the increasing molarity of aromatic alcohol solution which is associated with the stiffening effect of the chains. The results from MD showed a higher load carrying capability of polymer chains with the increasing molarity of AA solution. As observed, the dihedral angle stiffness and hydrogen bond characteristic contributes significantly to this chain stiffness in the presence of aromatic alcohol.

Experimental Section

Cross-linked chitosan thin film of ~80 µm thickness was prepared by solvent casting method where Chitosan solution (1.5% w/v) was prepared first by dissolving 150 mg of CS powder in 10 ml of acetic acid (1% v/v). Glutaraldehyde is used as a cross-linker and it is added to the already prepared CS solution in order to obtain a cross-linked film. The solution was stirred by keeping over a hot plate magnetic stirrer at ~ 45° C for 2 hours forming a homogenous solution. Rectangular size of 0.15 cm x 0.7 cm dimensions is applied for folding studies. This dry film was placed on water and aromatic alcohol (AA) solution of increasing concentration separately to study the reversibility and irreversibility of folding behaviour. For Dilelectric Spectroscopic Experiment, film of 20 mm diameter was soaked in AA solution of varying molarity for about 5 min till it reaches saturation. For molecular dynamics simulation study, five models i) a single chain chitosan polymer (CS), ii) chitosan chain solvated in water (CS-W), chitosan chain solvated in a mixture of water and AA solution of varying molarity, i.e. iii) 2M (CS-2M), iv) 10M (CS-10M) and v) 20M (CS-20M) were built and studied. For the mechanism study, a single polymer chain of chitosan consisting of 75 repeating units was built using Material Studio 6.0[36] and pulled applying spring constant of k= 7 kcal/mol/Å^2 and pulling velocity v = 0.5 Å/ps. The details of the methodology is given in Supplementary document (S.1).

Acknowledgements

The authors gratefully acknowledge the P.G. Senapathy Center for Computing Resource, IIT Madras, for providing the computational resources.

Notes and references

1 Zhang, K.; Geissler, A.; Standhardt, M.; Mehlhase, S.; Gallei, M.; Chen, L.; Marie Thiele, C. *Scientific reports* 2015, **5,** 11011.
2 Kempaiah, R.; Nie, Z. *Journal of Materials Chemistry B* 2014, **2** (17), 2357.
3 Chen, M.-C.; Tsai, H.-W.; Chang, Y.; Lai, W.-Y.; Mi, F.-L.; Liu, C.-T.; Wong, H.-S.; Sung, H.-W. *Biomacromolecules* 2007, **8** (9), 2774–2780.
4 Li, X.; Serpe, M. J. *Advanced Functional Materials* 2014, **24** (26), 4119–4126.
5 Mirfakhrai, T.; Madden, J. D. W.; Baughman, R. H. *Materials Today* 2007, **10** (4), 30–38.
6 Ye, C.; Nikolov, S. V; Geryak, R. D.; Calabrese, R.; Ankner, J. F.; Alexeev, A.; Kaplan, D. L.; Tsukruk, V. V. *Applied Materials and Interfaces* 2016**, 8**, 17694–17706.
7 Athas, J. C.; Nguyen, C. P.; Zarket, B. C.; Gargava, A.; Nie, Z.; Raghavan, S. R. *ACS Applied Materials and Interfaces* 2016, **8** (29), 19066–19074.
8 Martinez, R. V.; Branch, J. L.; Fish, C. R.; Jin, L.; Shepherd, R. F.; Nunes, R. M. D.; Suo, Z.; Whitesides, G. M. *Advanced Materials* 2013, **25** (2), 205–212.
9 Malachowski, K.; Jamal, M.; Jin, Q.; Polat, B.; Morris, C. J.; Gracias, D. H. *Nano Letters* 2014, **14**, 4164–4170.
10 Lu, T.; Zhu, S.; Chen, Z.; Wang, W.; Zhang, W.; Zhang, D. *Nanoscale* 2016, **8**, 10316–10322**.**
11 Chen, J.-K.; Chang, C.-J. *Materials* 2014, **7** (2), 805–875.
12 Reineke, T. M. *ACS Macro Letters* 2016, **5** (1), 14–18.
13 Lai, W.; Cheung, H. *Nanoscale* 2016, **8**, 517–528.
14 Mcdonald, T. O. *Nanoscale* 2017, **9** (19), 6302–6314.
15 Jeong, J.; Cho, yigil; Lee, S. Y.; Gong, X.; Kamien, R. D.; Yang, S.; Yodh, A. *Soft Matter* 2017, **13**, 956-962.
16 Liu, Y.; Boyles, J. K.; Genzer, J.; Dickey, M. D. *Soft Matter* 2012, **8** (6), 1764–1769.

View Article Online
DOI: 10.1039/C8SM00042E

17 Rath, A.; Mathesan, S.; Ghosh, P. *Soft Matter* 2016, **12** (45), 9210–9222.
18 Ionov, L. *Advanced Functional Materials* 2013, **23** (36), 4555–4570.
19 Stoychev, G.; Guiducci, L.; Turcaud, S.; Dunlop, J. W. C.; Ionov, L. *Advanced Functional Materials* 2016, **26,** 7733-7739.
20 Wong, W. S. Y.; Li, M.; Nisbet, D. R.; Craig, V. S. J.; Wang, Z.; Tricoli, A. *Science Advances* 2016, **2**, 417.
21 Danielson, C.; Mehrnezhad, A.; YekrangSafakar, A.; Park, K. *Soft Matter* 2017, **13**, 4224-4230.
22 Sun, Y.; Sai, H.; Spoth, K. A.; Tan, K. W.; Werner-zwanziger, U.; Zwanziger, J.; Gruner, S. M.; Kourkoutis, L. F.; Wiesner, U. *Nano Letters* 2016, **16**, 651-655.
23 Rath, A.; Mathesan, S.; and Ghosh, P., *Journal of the Mechanical Behavior of Biomedical Materials* 2015, **55**, 42–52.
24 Quijada-Garrido, I.; Iglesias-Gonzlez, V.; Mazon-Arechederra, J. M.; Barrales-Rienda, J. M. *Carbohydrate Polymers* 2007, **68** (1), 173–186.
25 Silva, R. M.; Reis, R. L.; Mano, J. F. *Biomacromolecules* 2004, **5**, 2073–2078.
26 Bobritskaya, E.; Bobritskaya, E. I.; Castro, R. A.; Temnov, D. E. Thermoactivation and *Physics of the Solid State* 2013, **55**, 225-228**.**
27 Bobritskaya, E. I.; Castro, R. A.; A, G. Y.; Temnov, D. E. *Physics of the Solid State* 2013, **685**, 336–339.
28 Kumar-Krishnan, S.; Prokhorov, E.; Ramírez, M.; Hernandez-Landaverde, M. a; Zarate-Triviño, D. G.; Kovalenko, Y.; Sanchez, I. C.; Méndez-Nonell, J.; Luna-Bárcenas, G. *Soft matter* 2014, **10** (43), 8673–8684.
29 Nogales, A.; Ezquerra, T.; Rueda, D.; Martinez, F.; Retuert, J. *Colloid & Polymer Science*. 1997, **275**, 419–425.
30 Ghosh, P.; Katti, D. R.; Katti, K. S. *Biomacromolecules* 2007, **8** (3), 851–856.
31 Lorenzo, A. C.; Caffarena, E. R. *Journal of Biomechanics* 2005, **38** (7), 1527–1533.
32 Perrin, C. L; Nielson, J. B. *Annual Reviews in Physical Chemistry* 1997, **48**, 511-544.
33 Desiraju, G. R. *Accounts of Chemical Research* 1991, **24**, 290–296.
34 Jeffrey, G. A.; Takagi, S. *Accounts of Chemical Research* 1978, **27** (4), 264–270.
35 Mathesan, S.; Rath, A.; Ghosh, P. *Materials Science and Engineering C* 2016, **59**, 157–167.
36 Accelrys Software Inc. 2011, Materials Studio v 6.0.0.